Energy 270 (2023) 126897

Contents lists available at ScienceDirect

Energy

journal homepage: www.elsevier.com/locate/energy

Employing Taguchi method to optimize the performance of a microscale combined heat and power system with Stirling engine and thermophotovoltaic array

Wen-Lih Chen [a,b], Gaetano Currao [a,b], Yueh-Heng Li [a,b,*], Chien-Chun Kao [a]

[a] Department of Aeronautics and Astronautics, National Cheng Kung University, Tainan, 701, Taiwan, ROC
[b] International Bachelor Degree Program on Energy, National Cheng Kung University, Tainan, 701, Taiwan, ROC

ARTICLE INFO

Handling Editor: G Chicco

Keywords:
Microscale heat and power system
Taguchi method
Stirling engine
Thermophotovoltaic
Biosyngas

ABSTRACT

This study proposes a biosyngas-fueled power system, which is a fusion between a micro-thermophotovoltaic (micro-TPV) system and a Stirling engine. The combustor in the micro-TPV is a coaxial tube made of platinum. Biosyngas was simulated using different compositions of H_2 and CO mixture. The H_2/CO/air mixture was delivered to the inner channel of the micro-TPV combustor, while the CH_4/air mixture was delivered to the outer channel. This study realized a micro-CHP system with a combustion-driven TPV cell array, and a Stirling engine-driven power generation system. This micro-CHP system harvests energy generated through thermal radiation from the reactor's surface as well as thermal energy from hot flue gas. The results indicate that the overall efficiency of the biosyngas-fueled micro-CHP system was strongly dependent on fuel composition, fuel/air ratio, and flowrate mixture. Thus, Taguchi method was employed to find optimal operative conditions; the highest efficiency was achieved under a biosyngas composition of 80% CO and 20% H_2, with a flow velocity of 6 ms^{-1}, and an equivalence ratio of 1.2, and its corresponding overall efficiency reached 43%, incorporating 0.84 W electricity output by TPV cell array, 3.25 W electricity output by Striling engine-driven power generation system, and 325.5 W of water energy gained.

1. Introduction

Agriculture and animal husbandry are considered to be the main income sources for remote villages. However, agricultural activities produce great quantities of agricultural waste and animal manure that can be categorized as biowaste [1,2]. Due to the rapid growth in population, waste from food processing and manufacturing, and ineffective grocery inventory have increased significantly and reached unprecedented levels [3]. Current bio refinery technology is able to convert these biomass wastes into valuable products such as biofuels or bio-oils [4]. For instance, bioelectricity is a form of power generation which relies on the fermentation of organic waste to produce biosyngas [5], it also poses almost no impact on atmospheric CO_2 concentration [6]. Therefore, slaughterhouses can convert municipal solid waste and animal manure into useable bioenergy. Due to the listed benefits, several countries have extensively used bioenergy including biogas, biodiesel, bio-alcohol, and syngas, at a commercial level [7,8].

Gasification is one of the promising clean technologies for producing syngas through thermochemical conversion. Normally the products of gasification include H_2, CO, and CH_4, but the output of the gasifying product also depends on the chemical composition of the feedstock, operational conditions, design of the gasifier, and the gasifier agent mixture [9]. Syngas can subsequently be used for power generation using internal combustion engines or gas turbines [10]. Syngas applications have been tested through several simulations and experiments to investigate the stabilization of the combustion reaction on a microscale. Al-attab and Zainal [11] built a combined syngas microscale gas turbine. The results revealed that NOx and CO emissions were below 250 and 15 ppm respectively, and that the overall system efficiency reached a maximum of 37.8% with a thermal output of 34 kW. Li and Kuo [12] explored the oxygen-enriched combustion behavior [49] of torrefied waste wood pellets in a fluidized bed. The resuls demonstrated that the degree of torrefaction of the biomaterials had the strongest influence on the total combustion efficiency of the fluidized bed, and bed temperature and oxygen concentration were equally important. But, oxygen inlet position had the weakest influence on combustion efficiency.

A combined heat and power system (CHP) is typically used to

* Corresponding author. Department of Aeronautics and Astronautics, National Cheng Kung Univ., Tainan, 701, Taiwan, ROC.
E-mail address: yueheng@mail.ncku.edu.tw (Y.-H. Li).

https://doi.org/10.1016/j.energy.2023.126897
Received 25 April 2022; Received in revised form 30 January 2023; Accepted 6 February 2023
Available online 8 February 2023
0360-5442/

Nomenclature

C_p	Specific heat of gas kJkmol^{-1}K^{-1}
C_w	Specific heat of water kJkmol^{-1}K^{-1}
ECI	Energy conversion index %
EPI	Electric power index %
E_{TPV}	Electricity output by TPV W
E_{SE}	Electricity output by SE W
$\overline{E}_{TPV}$	Normalized electricity output by TPV %
$\overline{E}_{SE}$	Normalized electricity output by SE %
E_x^{ch}	Chemical exergy J
E_x^{ph}	Physical exergy J
h_e	Enthalpy outlet kJkg^{-1}
h_i	Enthalpy inlet kJkg^{-1}
MW	Molecular weight kgkmol^{-1}
$\dot{m}$	Fuel mass-flow rate kgs^{-1}
Q_r	Radiation energy Wm^{-2}
Q_s	Sensible energy kJ
$\overline{Q}_r$	Normalized radiation energy %
$\overline{Q}_s$	Normalized sensible energy %
R_u	Universal gas constant JK^{-1}mol^{-1}
s_e	Entropy outlet kJkg^{-1}K^{-1}
s_i	Entropy inlet kJkg^{-1}K^{-1}
SNR	Signal to noise ratio
SNR_{avg}	The mean value of SNR
SNR_{opt}	SNR at the optimal level
T_0	Ambient temperature K
$\dot{W}$	Net power output W
x	Mole fraction

Greek

η	Overall efficiency %
η_E	Electricity efficiency %
η_I	Irradiation efficiency %
η_{SE}	Stirling engine efficiency %
η_{TPV}	TPV efficiency %

convert chemical energy from bio waste into electricity and heat [13,14] while maintaining a low production of CO_2 [15]. The excess heat can be effectively reintroduced into the thermodynamic cycle using an appropriate converter, thus reducing the greenhouse gas emission for the same amount of power output [16]. Additionally, compactness and low-cost maintenance make CHP system implementation ideal for the use in remote and poor areas. For example, Wu et al. [17] has designed a simple, unpressurized Stirling engine capable of generating 19 W of electric power with a medium temperature difference of 254 °C. Such temperature difference can be easily achieve by burning biomass fuel, which is abundant in rural areas.

Various CHP systems have been invented recently. Bianchi et al. [18] designed a micro-CHP, which comprises a CHP prime mover, an auxiliary boiler, and a thermal storage unit. The electricity produced from the CHP system could either be consumed within houses or offices or, if permitted by the grid management, sold back to the electric power grid. Chen et al. [19]examined the application of thermoelectricity (TE) generation in CHP systems with special focus on efficiency and CO_2 abatement. Yin et al. [20] analyzed four CHP systems using biogas for energy demands of a cassava starch plant. Assessment results indicated that CHP system with reciprocating internal-combustion engine obtained the best profit, followed by CHP with micro turbine, CHP with boiler/turbines, and CHP common system.

Solar thermal energy is extensively used for power generation [21,22] or water heating system [23]. The efficiency levels of solar thermal collectors or photovoltaic systems are typically between 1% and 10% [19]. Despite the low energy conversion efficiency, solar energy is widely harvested in conjunction with CHP systems in several ways [24]. Solar-thermal-driven CHPs are economically and technically attractive in aspects of off-grid renewable power and heat cogeneration. However, the intermittency of solar energy deteriorates the reliability and flexibility of the power system and defers the development of renewable energy-driven CHP systems. Wu and Han [25] designed solar-aided CHP system to preheat both feedwater and reheated steam, achieving the highest annual solar-to-electricity efficiency and the lowest levelized cost of energy.

Although combustion-driven TPV systems [26–28] have several advantages, for example, no moving parts and high reliability, they also have certain limitations such as restriction of photovoltaic effect and combustion instability [29]. An appropriate design of the combustor and emitter is strongly associated with the overall efficiency and life expectancy of the TPV system [30,31]. In addition, the spectral distribution of emission depends on specific materials [14]. Thus, a selective emitter emitting narrowband thermal radiation, which is appropriate for the conversion to electrical power through a TPV array, is required. For example, selective emitters must operate at high temperatures, hence materials with a high melting point are required. Higher-temperature tantalum [15] and tungsten [29] have been proposed to enhance thermal emittance. Optimal design for a selective emitter can result in high emittance, which overlaps with the bandgap of the PV cell while having low emittance for wavelengths outside the bandgap. Yeng et al. [32] optimized a broadband-wavelength selective emitter that possessed 86% of the wavelength range of operation. In order to address the resulting problems of low overall efficiency and low combustion integrity, an alternative approach is to integrate the TPV system with other types of power generation sources. For example, Qui and Hayden developed a novel combined power system using a TE and a TPV system [33]. A burner was used for heating a thermal emitter, while the exhaust heat was directly delivered to the hot junction of the TE system. Two emitters, made of SiC, were set on both sides and heated until incandescence. A filter was placed between the emitter and the PV array, reflecting out-of-band radiation back to the emitter. The total thermal input energy was 8260 W, and the electricity efficiency of the overall system reached 5.2%, with 1.5% from the TPV system and 3.7% from the TE system. Furthermore, the TPV system can be combined with a conventional boiler to recover more energy waste. The concept of TPV integrated with a boiler was proposed for a cogeneration system [34]. The electrical power of the TPV system could reach the range of 158 W–246.4 W depending on the fuel input and the corresponding efficiencies spanned from 1.86% to 2%. The overall efficiency, which is the sum of the thermal and electrical efficiencies, approached 85.4%.

An open issue is that the combination of the CHP system may cause one of the hybrid power systems to be the consequence of lower performance once it operated under an improper condition. To maximize the overall power output of the integrated system, it is necessary to improve the overall efficiency of the CHP system by tuning the performance of individual power modules. Taguchi method can not only provide quality examination but also assess the importance of the operational parameters regarding overall performance. Huang et al. [35] investigated coal blended with torrefied Miscanthus biochar by Taguchi method. By using the orthogonal array, they could determine the optimization conditions for the blended fuel. Comakli et al. [36] used this method to investigate the optimal conditions that affect the COP and heat pump efficiency by using R22/R404A mixtures. Coskun et al. [37] conducted a quality examination by using Taguchi method and artificial neural network (ANN) prediction on waste heat recovery

application to obtain significant control parameters and optimum conditions. The results based on both methods were consistent with one another.

Some studies have focused on establishing a micro-CHP using different independent systems. In terms of waste heat recovery, the overall efficiency can be improved considerably; however, very few studies have optimized the CHP system. According to the literature [8,38], syngas can be produced by fossil fuel as well as the gasification of agricultural waste and natural resources. The main components of syngas, CO and H_2, can be stabilized on a micro-combustor with the assistance of a platinum catalyst [51]. Using syngas, the homogeneous reaction on a platinum surface can catalyze CH_4 in a small area; that is, it can serve as an emitter for the TPV system due to the high brightness of the platinum combustion chamber. Some research has indicated that H_2 and CO can have a surface reaction over a Pt surface under a fuel-lean condition. Hayes [39] built an experimental system and compared the results with the simulation. They studied the reaction between H_2 and CO on a supported platinum catalyst under a fuel-lean condition and indicated that the enhancement of CO light-off temperature poses a substantial effect on the low concentration. Li et al. [39] showed another aspect of the interaction between H_2 and CO over the platinum surface in a small region with three different geometries. The catalytic surface was separated into three forms of the same length. Three mixture ratios, 30%H_2 +70%CO, 50% + 50%CO, and 70%H_2 +30%CO, were used to investigate the varying amounts of syngas composition. Due to the high reaction rate of both fuels over the platinum surface, three types of mixtures could reach a high conversion rate inside the micro-combustor. Furthermore, CH_4 was tested under the same condition as those for H_2 and CO. However, with the assistance of H_2 and CO, heterogeneous and homogeneous reactions could be achieved inside the micro-combustor. The studies above have proven that platinum can work as a favorable catalyst for promoting syngas combustion on a microscale.

Based on previous studies [27,40,52], the high reaction rate of H_2 facilitates stable combustion of CH_4 inside a coaxial platinum tube through heterogeneous and homogeneous reactions. The latest study [40] pointed out the operational range of the flame behavior of CO/H_2/air mixture is sustainable in a micro combustor in terms of the variation of velocity, the equivalence ratio, and the mixing ratio. It is readily to see that the reaction is dominated by CO concentration under a fixed velocity and stochiometric condition. However, more details on the efficiency and other index related to the CHP system should be the subjects for further investigation. In this study, the same combustor was continuously used as an emitter for the micro-TPV system. Syngas with different mixture ratios of H_2 and CO will be used as fuel for the micro-combustor. Flame situations occurring on the micro-combustor will be systematically discussed under various conditions. The electricity output and overall efficiency of the power generation can be determined individually. Furthermore, to achieve higher performance of the CHP system, Taguchi method will be adopted to optimize various parameters, such as equivalence ratio, flow velocity, and mixing ratio through syngas, of the combustion in the combustor. Several conditions of different mixing ratios between H_2 and CO will be selected to discover the effect of syngas through this system. To improve the system's efficiency, three different parameters with three levels will be analyzed by Taguchi method. An orthogonal array will be used to find the most influential parameters which determine the optimal condition. Since the cooling water of the Stirling engine will be heated by the engine's waste heat and become hot water after a period of engine operation, the present system can be regarded as a CHP system. However, compared to the conventional CHP technique, the present technique adopts two different electricity-generation mechanisms; hence, it can potentially generate more electricity. In this CHP system, the micro-combustor is the most important device because it is the power source of the entire system. Therefore, the main goal of this study is to find the operational conditions of the micro-combustor to enable the system to achieve optimal performance in terms of one of three objectives, energy conversion, electrical power output, or exergy conversion.

2. Experimental setup

2.1. Microscale combustor and measurement system

As shown in Fig. 1, The inner channel of the present micro-TPV combustor is a cylindrical tube made of platinum with dimensions of 5.3(ID) × 6(OD) × 40(L) mm. The support is a steel tube with dimensions of 4(ID) × 5.3 (OD) mm. The platinum tube combustor is surrounded by a quartz tube with dimensions of 8(ID) × 10(OD) × 70(L) mm, thus forming the outer channels of the combustor. At 5 mm from the steel base, eight orifices with a diameter of 1 mm are used to enhance flame stabilization [26,41].

As shown in Fig. 2, the mixture of H_2, CO, and air was delivered to the inner channel, while the mixture of CH_4 and air was delivered to the outer channel. The inner channel mixture was subjected to a parametric study, but the concentration of CH_4 was fixed. All flow meters were calibrated with the dry flow calibrator (Definder 220, Brandt Instruments, USA), resulting in uncertainty below 1% in all the mass flow readings.

A digital camera (NIKON D80, NIKON Corporation, Japan) with an exposure time of 1/400s and an aperture of F5.6 was used to film the flame behavior. The irradiation emitted from the micro TPV was measured by an integrating sphere surrounding the TPV and coated with MgO for more uniform light distribution. During the irradiation measurement, the quartz tube was replaced by a longer one (150 mm) to prevent high-temperature exhaust diffusing into the sphere. A fiber, the gray line in Fig. 2, was connected between the integrating sphere and the spectrometer (spectral wavelength ranges from 200 to 1100 nm, USB2000, Ocean Optics, USA), permitting the measurement of radiation flux. Finally, a gas analyzer (VarioPlus, MRU Instrument, Germany) was connected at the exhaust port of the micro-TPV combustor to analyze the flue gas emission (O_2, CO, CO_2, and NO_x) for estimating the efficiency of the combustion.

2.2. Combined heat and power system

Fig. 3 shows a schematic of the CHP system. Since the radiation intensity spectrum is within 1100–1400 nm [27], a PV array of 2 × 12 GaSb cells (JX Crystal, USA) with an absorption spectrum between 400 and 1800 nm was employed. The specifications of the PV cell array are as follows: open-circuit voltage, 23.023 V; short-circuit current density, 2.9875 A/cm^2; and fill factor, 0.733. The maximum open-circuit voltage and short-circuit current density are 17.769 V and 2.5754 Acm^{-2}, respectively. This leads to the maximum power density of 45.763 Wcm^{-2}. To measure the power of the TPV power system, an electric load

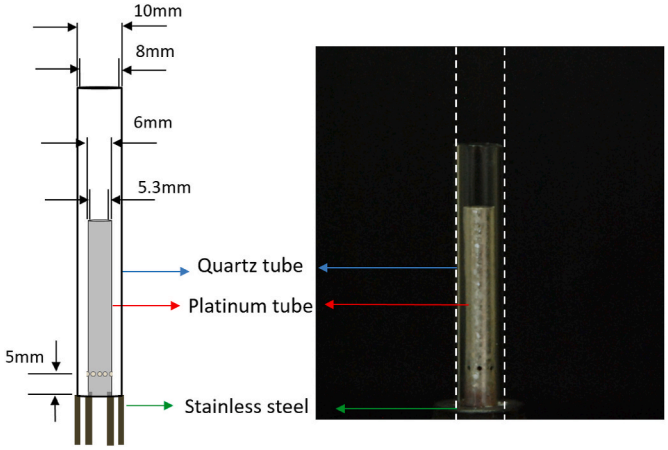

Fig. 1. Photograph of the micro-TPV combustor with dimensions.

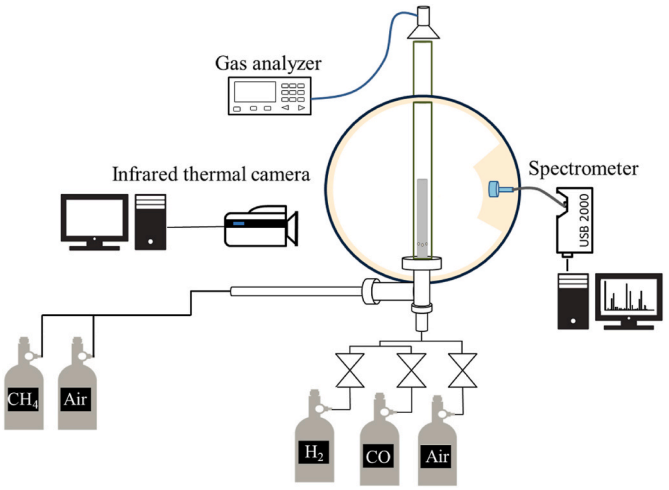

Fig. 2. Schematics of the experimental apparatus.

device (331D, Prodigit, Taiwan) was employed to measure the power output. This electrical load is controlled by using a computer equipped with GPID and RS232, while four modes, namely constant resistance, constant voltage, constant power, and short circuit, are used to detect five components. The selective resistance is 0.5–101.35 Ω with a total selective resistance of 90 Ω.

In Fig. 3, a water-cooled unpressurized γ-type Stirling engine, placed on top of the micro-combustor, is employed for converting the thermal energy of flue gas to electricity by driving a generator. Some important geometrical and operational parameters of the Stirling engine are listed in Table 1. Two pipes connect the Stirling engine water-tank, located below the flywheel, with two larger water tanks situated higher than the engine's water tank. This allows thermal syphon to take place, and cooling water can then circulate to the engine automatically with mass flow rate of 0.12 kg/s.

The Stirling engine is placed above the micro-TPV combustor so that the exhaust gas with high temperature can serve as the heat source for the Stirling engine. A generator is connected to the engine via the flywheel shaft to perform the mechanical-to-electric power conversion. A DC-to-DC converter is needed to further convert the variable-voltage electricity from the generator to constant 5-V electricity for powering commonly used appliances. The efficiency of this two-stage energy conversion (generator and converter) is approximately 50%.

3. Methodology

The following sections discuss the methodology adopted to identify the optimal operative conditions while minimizing the number of tests.

3.1. Taguchi method

Taguchi method [42] is an optimization approach that can reduce the number of tests for finding the optimal operative conditions. For instance, if three parameters and four levels are adopted to find the optimal operative conditions, 81 (3^4) experimental runs are required for the full factorial. However, using Taguchi method through an orthogonal test array, the number of runs can be reduced to 9. In this work, the quality indicator is expressed in terms of signal-to-noise ratio (SNR) [43] as follows:

$$SNR = -10 \times log\left[\frac{\sum_{i=1}^{n}\left(\frac{1}{y_i}\right)^2}{n}\right] \quad (1)$$

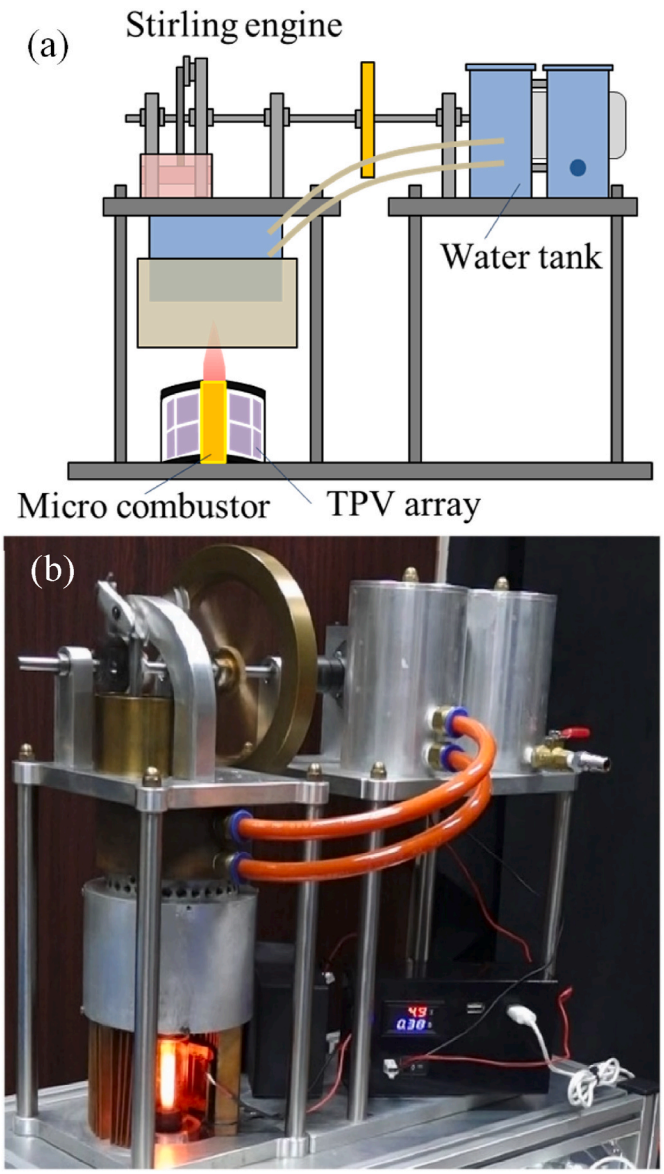

Fig. 3. (a) Micro-CHP system assembled with a TPV cell array, Stirling engine, and power generator. (b) Photo of micro-CHP system assembled with a TPV cell array, Stirling engine, and power generator [40].

Table 1
The values of important geometrical and operational parameters of the current Stirling engine.

Power-cylinder diameter (m)	0.050
Displacer-cylinder diameter (m)	0.060
Displacer diameter (m)	0.059
Power-piston stroke (m)	0.032
Displacer stroke (m)	0.032
Displacer-cylinder height (m)	0.140
Displacer height (m)	0.106
Compression ratio	1.158
Max. rotation speed (rpm)	1600.0
Max. mechanical power output (W)	12

where y_i is the performance parameter measured for the i-th test, and $n = 9$ is the total number of tests. The SNR is relative to a single Taguchi index or performance parameter.

3.2. Choice of the performance parameters

In this work, three indices are employed to characterize the micro-CHP system, namely energy conversion index, electrical power index, and exergy index.

The energy conversion index is derived from the energy flow balance analysis of the micro-CHP system. Based on energy conservation, the energy released from burning fossil fuel is equivalent to the summation of thermal radiation from the emitter, sensible heat from flue gases, and energy loss. Thermal radiation, or irradiation, is the main source for the TPV cell array to convert heat to electrical power, whereas the sensible heat of flue gas is used as an external heat source for the Stirling engine. There are two combustion modes coexisting in the micro-reactor, which are surface reaction and gas reaction. The surface reaction over the catalytic reactor pertains to a heterogeneous reaction, while the gas combustion inside the combustion chamber is a homogeneous reaction. The intensity of the heterogeneous reaction over the catalytic reactor is associated with the intensity of incandescent illumination from the emitter. Similarly, the temperature of flue gas is proportional to the combustion efficiency of a homogeneous reaction. Consequently, the competition between heterogeneous and homogeneous reactions is associated with the power contribution of the TPV cell array and Stirling engine. Thus, the energy conversion index (ECI) is proposed and defined as:

$$\mathrm{ECI} = \overline{\mathrm{Q}}_{\mathrm{r}} + \overline{\mathrm{Q}}_{\mathrm{s}} \tag{2}$$

where $\overline{\mathrm{Q}}_{\mathrm{r}}$ and $\overline{\mathrm{Q}}_{\mathrm{s}}$ are normalized radiation and sensible energy from the flue gas, respectively. Employing the energy conversion index entails examining the contributing factor of various energy forms (radiative intensity or high temperature of flue gas) to the micro-CHP system fueled with bio-syngas.

The electrical power index (EPI) is proposed and defined as:

$$\mathrm{EPI} = \overline{\mathrm{E}}_{\mathrm{TPV}} + \overline{\mathrm{E}}_{\mathrm{SE}} \tag{3}$$

where $\overline{E}_{TPV}$ and $\overline{E}_{SE}$ are normalized electrical power generated by the TPV cell and the Stirling engine-driven power generation system, respectively. $\overline{E}_{TPV}$ and $\overline{E}_{SE}$ were normalized by dividing each value of electrical power E_{TPV} and E_{SE} with the maximum value observed in all cases.

The last Taguchi index is related to exergy, which is a measure of the maximum capacity of a system for performing useful work as it proceeds to a specified final state in equilibrium with its surroundings. Exergy can be calculated based on two separate and independent physical and chemical exergies. Physical exergy E_x^{ph} is determined as the working gas assumed to be ideal gas, while chemical exergy is dependent on the fuel type and chemical reactions [44]. For each gas component, physical exergy on a per-unit-mass basis is defined as:

$$E_x^{ph} = (h_i - h_e) - T_0(s_i - s_e) \tag{4}$$

where h_i and h_e are the specific enthalpies of inlet and outlet flows; s_i and s_e are specific entropies of inlet and outlet flows; T_0 is the ambient temperature. h_i and h_e are calculated by the following equations:

$$(h_i - h_e) = \sum_i MW_i \int_{T_i}^{T_e} C_{p,i}\,dT \tag{5}$$

$$(s_i - s_e) = \sum_i MW_i \int_{T_i}^{T_e} \frac{C_{p,i}}{T}\,dT \tag{6}$$

where MW_i is molecular weight of species i, and $C_{p,i}$ is the constant pressure-specific molar heat capacity of species i, which is given in Table 2 [45].

Table 2
Constant pressure-specific heat capacity of some species.

Species	C_p [kJ/kmol-K]
N_2	$39.06 - 512.79 \times \left(\frac{T}{100}\right)^{-1.5} + 1072.7 \times \left(\frac{T}{100}\right)^{-2} - 820.4 \times \left(\frac{T}{100}\right)^{-3}$
O_2	$25.48 + 1.52 \times T \times 10^{-2} - 0.7155 \times T^2 \times 10^{-5} + 1.312 \times T^3 \times 10^{-9}$
H_2	$29.11 - 0.1916 \times T \times 10^{-2} + 0.4003 \times T^2 \times 10^{-5} - 0.8704 \times T^3 \times 10^{-9}$
CO	$28.16 + 0.1675 \times T \times 10^{-2} + 0.5327 \times T^2 \times 10^{-5} - 2.222 \times T^3 \times 10^{-9}$
CH_4	$18.89 + 5.024 \times T \times 10^{-2} + 1.269 \times T^2 \times 10^{-5} - 11.01 \times T^3 \times 10^{-9}$

Table 3 shows the molar fraction and molar exergy of the pure species used in this study. The molar exergy of the pure component, under conditions of 298.15 K and 101.3 kPa, and the chemical exergy E_x^{ch} can be obtained as follows [44]:

$$E_x^{ch} = R_u T_0 \ln x_i \tag{7}$$

where $R_u = 8.314\ \mathrm{Jmol^{-1}K^{-1}}$, $T_0 = 298.15$ K, and x_i is its molar fraction in the environment.

By multiplying the flow rate of each fuel component, the total exergy can be determined. The equation of exergy efficiency η_{ex} can be expressed as [44]:

$$\eta_{ex} = \frac{\dot{W}}{\sum_i (m_i \times E_{x_i})} \tag{8}$$

where the denominator is the total input exergy for each component and $\dot{W}$ is the net power output.

3.2.1. Effect of mixing ratio through the inner channel

Fig. 4 shows the photo of combustion behavior under different mixing ratios of H_2:CO with a fixed velocity of 5 $\mathrm{ms^{-1}}$ and the stoichiometric condition. For the case with higher H_2 content, the brighter incandescent section of the platinum reactor is concentrated at the upstream of the micro-TPV combustor. When the CO content increased, the incandescent part expanded to the lower part of the micro-TPV combustor, which increased the power output of the PV array.

Table 4 shows different conditions of different mixing ratios between H_2 and CO with a fixed velocity of 5 $\mathrm{ms^{-1}}$ and the stoichiometric condition. Irradiance is measured by the integrating sphere. Electricity generated by TPV and Stirling engine was measured separately by an electrical load and a power generator. Water energy gained per second is measured by the water tank for cooling the Stirling engine and calculated based on the equation, $H = \dot{m}\, C_w \Delta T$. Here, $\dot{m}$ is the mass flow rate of water, 0.12 $\mathrm{kgs^{-1}}$, C_w is the specific heat of the water, and ΔT is the temperature change after 10 min of operation. Efficiency was calculated as the total output energy, including the energy absorbed by the cooling water, divided by total input energy.

Cases shown in Table 4 are one high H_2 concentration condition (80%H_2+20%CO) and one high CO concentration condition (20%H_2 + 80%CO). When the fuel composition changed to a higher CO content, the irradiance increased from 43,290 to 53,381 $\mathrm{Wm^{-2}}$, which is a remarkable 23.3% increase. Also, the electricity output (E_{TPV}) increased by 22.5% when the CO content increased in the inner channel. Moreover, both the electricity output (E_{SE}) and water energy gained per second from the Stirling engine increased by 18.3% and 16%,

Table 3
Molar exergy of pure species under 298.15 K and 101.3 kPa conditions [46,47].

Substance	Molar fraction	Molar exergy [$\mathrm{kJmol^{-1}}$]
N_2	0.7651	0.66
O_2	0.2062	3.9
H_2	NA	236
CO	NA	275
CH_4	NA	831

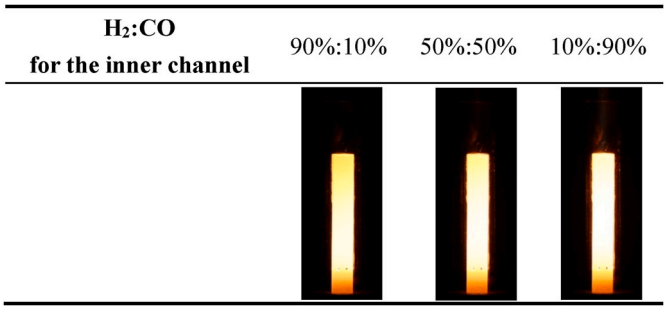

Fig. 4. Photos of combustion behavior with different mixing ratios of H_2:CO under a fixed velocity at 5 ms^{-1} and stoichiometric condition.

Table 4
Performance and efficiency of micro-CHP system under two different mixing ratios.

H_2:CO in inner channel	Irradiance [W/m^2]	E_{TPV} [W]	E_{SE} [W]	Water energy gained per second [W]	Efficiency [%]
80%:20%	43,290	0.8	2.3	262.5	33.65%
20%:80%	53,381	0.98	2.72	304.5	40.23%

respectively. In terms of efficiency, it approximately increased 20% due to the increase in the power output and the decrease in total energy input.

3.2.2. Effect of velocity through the inner channel

With more energy input to the micro-TPV combustor, it is expected that more energy should be generated by the system. For example, by fixing the mixing ratio of H_2:CO to 50%:50% and under stoichiometric condition, the total input energy is 622.14 W when flow velocity is 4 ms^{-1}. Once the velocity increases to 5 ms^{-1}, the total energy input is 777.68 W, resulting in a 25% increase of input energy. However, the power output may not be proportional to the input energy, and there exists considerable energy loss because of the small scale of the system.

Fig. 5 shows the combustion behavior at different velocities of inner fuel/air mixtures under the stoichiometric condition and fixed mixing ratio of 50% H_2+50%CO. It can be noted that lower flow velocity gives rise to dimmer red color emitting from the micro TPV combustor. As the flow velocity increases, meaning an increase in input energy, higher luminosity emanates from the micro-TPV combustor.

Flow velocity can pose significant effect on input energy. Table 5 shows the system's performance versus velocity with H_2:CO fixed at 50%:50% and stoichiometric condition. The maximum flow velocity of the micro-TPV combustor is 7 m s^{-1}. Once the flow velocity is higher than 7 m s^{-1}, the flame will blow off due to the low burning velocity of the CO fuel. Therefore, we limited the maximum flow velocity at 6 m s^{-1} in the experiment. It is noticeable from Table 5 that irradiance increases 50% as the flow velocity increased from 4 ms^{-1} to 6 ms^{-1}. The increase in irradiance resulted in a significant improvement (54%) on electricity output by the PV array. The improvement due to velocity increase also appeared in the Stirling engine's performance. The electric power increased from 1.98 W to 3.1 W, which is a 36.6% improvement; and the water energy gained per second increased 83.3%. Although there is considerable improvement on the performance of both TPV and Stirling engine, the efficiency only increased 22%. The main reason is that the percentage of the increase in the input energy is even larger. It increased from 622.15 W to 933.22 W, which is a 50% increase as the velocity increased.

Table 5
Performance and efficiency of micro-CHP system under two different velocities.

Velocity [m/s]	Irradiance [W/m^2]	E_{TPV} [W]	E_{SE} [W]	Water energy gained [W]	Efficiency [%]
4	32,150	0.59	1.98	188.37	30.7
6	49,231	0.91	3.1	345.35	37.44

3.2.3. Effect of equivalence ratio through the inner channel

The equivalence ratio is another important parameter to be discussed. It could increase the power generated by PV cell or Stirling engine. Higher equivalence ratio may result in incomplete combustion inside the micro combustor; however, when unburned fuel flows outside the quartz tube, a tail flame would boost the power of the Stirling engine, increasing the overall power output of the micro-CHP system. Fig. 6 shows the combustion behavior of different equivalence ratios with velocity fixed at 5 ms^{-1} and a mixing ratio of 50%H_2+50%CO.

Table 6 shows the equivalence ratio effect on the performance of the micro-CHP system with flow velocity fixed at 5 ms^{-1} and the ratio of H_2: CO in the inner channel fixed at 50%:50%. The increase of the equivalence ratio only results in a moderate rise in input energy, and consequently, moderate improvement on micro-CHP system's performance. Table 6 shows that as the equivalence ratio increased from 0.8 to 1.2, the irradiance only increased slightly from 42,297 W/m^2 to 45,057 W/m^2, which is a mere 7% increase. This slight increase in irradiance gave rise to a 6% increase in PV array power from 0.78 W to 0.83 W. The performance of the Stirling engine is also moderately improved, as electric power and water energy gained per second increased from 2.5 W to 2.76 W and 272.09 W–293.02 W respectively. Although all the power output increased with the increase in equivalence ratio, the efficiency has decreased. Unlike the velocity parameter that posed improvement on both the system's power output and efficiency, the equivalence-ratio parameter only improved power output but posed negative effect on

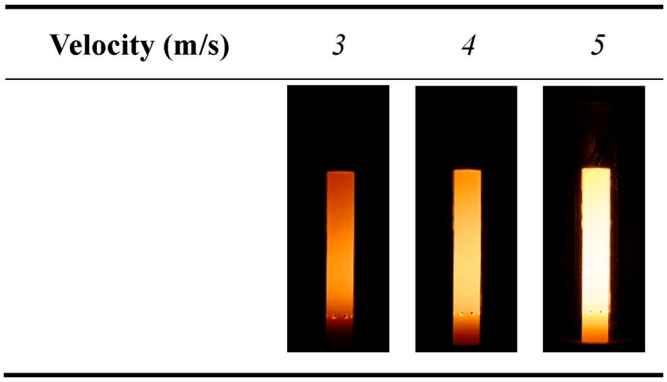

Fig. 5. Combustion behavior at different velocities of inner fuel/air mixtures with the stoichiometric condition and fixed mixing ratio of H_2: CO at 50%:50%.

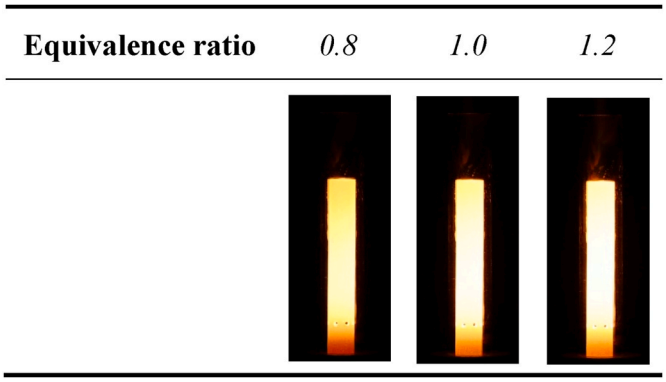

Fig. 6. Combustion behavior of different equivalence ratios with the fixed velocity at 5 ms^{-1} and mixing ratio of H_2: CO at 50%:50%.

Table 6
Performance and efficiency of the micro-CHP system under two different equivalence ratios under a fixed velocity of 5ms^{-1} and a fuel composition of H_2: CO at 50%:50% in the inner channel.

Equivalence	Irradiance [W/m^2]	E_{TPV} [W]	E_{SE} [W]	Water energy gained [W]	Efficiency [%]
0.8	42,297	0.78	2.5	272.09	37.76
1.2	45,057	0.83	2.76	293.02	36.25

efficiency.

From the discussion above, we can tell that all parameters can significantly affect the power output of the micro-CHP system. Although the increase in equivalence ratio posed a negative effect on efficiency, it may have a positive effect under other conditions. The parametric study above is only intended to identify the most influential parameters for the micro-CHP system. An optimization study is needed to find the best combination of these parameters. Section 4 will optimize these parameters using Taguchi method on more experiments.

4. Optimization for overall efficiencies of micro-CHP

4.1. Selection of the optimization indicators

The three main parameters introduced above will vary within a specific range. The values of equivalence ratio considered here are 0.8, 1.0, and 1.2. The values of flow velocity are set at 4, 5, and 6 ms^{-1}, since higher speeds cannot be achieved with the current set-up. Three different mixing ratios will be tested, namely 80%H_2 and 20%CO, 20% H_2 and 80%CO, and 50%H_2 and 50%CO. Table 7 shows the orthogonal array L_9 (3^3), which effectively reduces the total of 27 experiment runs to 9 runs, reducing time and experimental costs.

4.2. Characteristic measurement of micro-TPV combustor

In the present Taguchi analysis, three parameters, namely hydrogen mole fraction, flow velocity, and equivalence ratio, with three levels are considered. To determine the optimal condition based on these indicators, the radiation intensity from the emitter, flue gas temperature, gas emission, and electrical power from the TPV system and Stirling engine-driven power system are measured. According to the L9 orthogonal array in Taguchi method, nine sets of conditions are required. Table 8 lists the combustion characteristics and power performance of the micro-combustor and micro-CHP system under different fuel/air conditions. Note that the measured values for each indicator may vary considerably. To equalize the dominance of the parameters, it is necessary to normalize the measured values before processing the signal-to-noise analysis. Taking the energy conversion index as an example, the lowest measured values of irradiance from the emitter and sensible energy from the flue gas temperature are 21,279 W/m^2 and 110.94 kJ respectively for case 1. In contrast, in terms of the maximum irradiance and flue gas temperature in case 3, the values are 52,951 W/m^2 for irradiance and 84.62 kJ for sensible energy of flue gas. The irradiance in case 3 is almost 2.5 times larger than that in case 1, but there is a 24% decrease in the sensible energy of flue gas. The magnitude of energy variation in irradiance and sensible energy of flue gas is obviously different, and leads to the influence of the parameter in large variation outweighing the other parameters. To mitigate this misjudgment, the irradiance and sensible energy can be normalized by dividing the maximal value of each parameter in the energy conversion index and electrical power index. For example, the value of radiation energy Q_r in case 1 is 21279 and divided by the maximum value of Q_r (52951) in Table 8. The normalized radiation energy $\overline{Q}_r$ is 0.4 as shown in case 1 of Table 9. Table 9 displays the normalized values for the optimal process with different indices.

Table 7
Experimental layout using an L_9 orthogonal array.

No.	H_2:CO	Velocity [m/s]	Equivalence ratio
1	80%:20%	4	0.8
2	80%:20%	5	1.0
3	80%:20%	6	1.2
4	50%:50%	4	1.0
5	50%:50%	5	1.2
6	50%:50%	6	0.8
7	20%:80%	4	1.2
8	20%:80%	5	0.8
9	20%:80%	6	1.0

4.3. SNR

Based on the results of the nine experimental sets, the SNR value for each indicator can be determined. For example, in case 1, Table 9 indicates normalized radiation and sensible energy of flue gas to be 0.4 and 1.0 respectively. Thus, by using Eq. (1), the SNR can be calculated as 2.92. Table 10 shows the SNR values for the three indicators. To obtain the energy conversion parameters, the mean of the SNR values at different levels is calculated. The H_2 mole fraction for cases 1–3 is fixed at 0.8. The mean SNR value is calculated as $\frac{1}{3}(2.93 + 4.99 + 5.69) = 4.54$.

The mean SNR value for each level can be calculated similarly. The results are shown in Table 11. To understand the main influence on the performance and efficiency of the micro-CHP system, the impact value of all parameters is determined by subtracting the maximum and minimum values of SNR at each level. A higher impact value ($SNR_{Max} - SNR_{Min}$) represents that the adjustment of the fuel condition can exert stronger influence on the performance of the micro-CHP system. According to the calculated results, the flow velocity has the strongest influence on the results. Higher energy input leads to higher performance. As shown in Table 11, the indicator of electrical power is influenced considerably more by the velocity than the other two parameters. However, in terms of the energy conversion index, the effect of the equivalence ratio is close to that of the velocity. Moreover, the mixing ratio is affected by the efficiency index. The heating value of CO is lower than that of H_2. Hence, an increase in the CO content in the inner channel results in lower input energy, and consequently, the efficiency of the micro-CHP system increases.

4.4. Confirmation experiment

The final step of Taguchi method is to validate the optimal conditions. The SNR value is predicted using the orthogonal array. The energy conversion indicator can be exemplified and calculated as follows [35, 48]:

$$SNR_{opt} = SNR_{avg} + (A_3 - SNR_{avg}) + (B_3 - SNR_{avg}) + (C_3 - SNR_{avg}) = 5.93 \quad (9)$$

In which SNR_{opt} is the mean of SNR values at the optimal level, while SNR_{avg} is the mean value of SNR. A_3, B_3, and C_3 are the maximum values of SNR of the H_2 mole fraction, velocity, and equivalence ratio respectively. The corresponding values are 5.04 for A_3, 5.47 for B_3, and 5.03 for C_3. Other optimal conditions are shown in Table 12.

To validate the accuracy of the results derived by Taguchi method, the optimal condition was tested, and the mean SNR values were determined. The error value of each indicator was determined by subtracting the SNR of the theoretical optimal value and experimental value. The error values for the indicators were less than 3% for three indicators, and as shown in Table 13, the exergy efficiency has a lower error value when the experimental result is compared to the prediction. This is due to higher amount of fuel and air, giving rise to higher exergy input. Yet, the increase in input exergy does not significantly increase

Table 8
Characteristic analysis of micro-combustor and micro-CHP system

No.	H_2 mole fraction	Velocity **[m/s]**	Equivalence ratio	Energy conversion		Electrical power		Exergy	
				Q_r [W/m^2]	Q_s [kJ]	E_{TPV} [W]	E_{SE} [W]	Input exergy [W]	Net power output [W]
1	0.8	4	0.8	21279	294.18	0.43	1.68	1036.68	47.31
2	0.8	5	1.0	43003	283.52	0.63	2.76	1332.33	71.09
3	0.8	6	1.2	52951	272.22	0.86	3.08	1628.89	84.24
4	0.5	4	1.0	35351	292.87	0.47	1.98	1066.68	47.65
5	0.5	5	1.2	45057	270.02	0.56	2.76	1367.55	73.52
6	0.5	6	0.8	44551	285.50	0.68	2.7	1558.58	81.18
7	0.2	4	1.2	39373	271.89	0.49	2.21	1095.33	52.9
8	0.2	5	0.8	42878	292.68	0.56	2.5	1307.97	70.76
9	0.2	6	1.0	49745	281.86	0.78	3.25	1608.17	89.33

Table 9
Normalization of characteristic analysis.

No.	H_2 mole fraction	Velocity **[ms^{-1}]**	Equivalence ratio	Energy conversion		Electrical power		Exergy	
				$\overline{Q}_r$	$\overline{Q}_s$	$\overline{E}_{TPV}$	$\overline{E}_{SE}$	Input exergy	Net power output
1	0.8	4	0.8	0.40	1.00	0.50	0.52	0.64	0.53
2	0.8	5	1.0	0.81	0.96	0.73	0.85	0.82	0.80
3	0.8	6	1.2	1.00	0.93	1.00	0.95	1.00	0.94
4	0.5	4	1.0	0.67	0.99	0.55	0.61	0.65	0.53
5	0.5	5	1.2	0.85	0.92	0.65	0.85	0.84	0.82
6	0.5	6	0.8	0.84	0.97	0.79	0.83	0.96	0.91
7	0.2	4	1.2	0.74	0.92	0.57	0.68	0.67	0.59
8	0.2	5	0.8	0.81	0.99	0.65	0.77	0.80	0.79
9	0.2	6	1.0	0.94	0.96	0.91	1.00	0.99	1.00

Table 10
SNR values of the nine experiments using three indicators.

No.	Energy conversion	Electrical Power	Exergy
1	2.93	0.15	7.79
2	4.99	3.98	9.02
3	5.69	5.79	9.19
4	4.42	1.26	7.81
5	4.95	3.52	8.72
6	5.16	4.20	8.72
7	4.44	1.94	8.31
8	5.13	3.05	8.87
9	5.56	5.61	9.39
Average	4.81	3.28	8.65

the net power output. In addition, the electrical power output has a close to 3% error. This might be because there is a significant change in luminous intensity by a small amount of CO addition. However, once the CO concentration dominates the inner fuel, the increase in light intensity is weakened. Nevertheless, higher efficiency and prediction can be determined through Taguchi method. We observed that with an increase in CO content in the inner channel, the overall efficiency can be increased. The outcomes of optimal operating conditions for the three indicators are identical. The overall efficiency under the conditions of velocity equal to 6 ms^{-1}, equivalence ratio of 1.2, and 80%CO+20% H_2 in the inner channel fuel reached 43%, incorporating $E_{TPV=0.84\ W}$, $E_{SE=3.25\ W}$, and water energy gained of 325.5 W.

5. Conclusion

In this study Taguchi method was applied, and three indicators, energy conversion, electrical power, and exergy conversion were proposed to examine their effects on the performance of a micro-CHP system. Three conditions with three levels were used to construct the orthogonal array of the experimental set. It was found that the optimal condition was the highest velocity with a higher equivalence ratio and low H_2 mole fraction. Meanwhile, the error value was lower than 3% for each index, proving the correctness of the optimal conditions. Once the velocity exceeds 6 ms^{-1}, flame will blow off under high CO content

Table 12
Optimal operating conditions for the three indicators.

Optimal condition	Energy conversion	Electrical power	Exergy
H_2 mole fraction	0.2	0.2	0.2
Velocity (m/s)	6	6	6
Equivalence ratio	1.2	1.2	1.2

Table 13
Validation of optimal combustion conditions.

	Energy conversion	Electrical power	Exergy
Theoretical optimal value	5.93	6.07	9.22
Experimental value	5.84	5.89	9.19
Error value (%)	1.57	2.97	0.33

Table 11
Impact value of three parameters for each indicator in three levels.

	Energy conversion			Electrical power			Exergy		
	H_2 mole fraction	*Velocity*	*Equivalence ratio*	*H_2 mole fraction*	*Velocity*	*Equivalence ratio*	*H_2 mole fraction*	*Velocity*	*Equivalence ratio*
L1	4.54	3.93	4.41	3.31	1.11	2.46	8.66	7.97	8.46
L2	4.84	5.02	4.99	2.99	3.52	3.62	8.42	8.87	8.73
L3	5.04	5.47	5.03	3.53	5.20	3.75	8.86	9.10	8.74
$SNR_{Max} - SNR_{Min}$	0.51	1.54	0.62	0.54	4.09	1.29	0.44	1.13	0.28

condition, which cannot be sustained inside the micro combustor. Furthermore, regarding fuel composition, the mixing ratio of H_2:CO is 20%:80%, which was tested by Taguchi method. In terms of the gasification product of syngas, the CO content may be under 90%. In this work, it is shown that for different H_2 to CO mixing rates, there could be a stable flame behavior through this system. Finally, the effect of increasing equivalence ratio became insignificant as the value of equivalence ratio has passed certain threshold. Therefore, it could be deduced that the optimized condition has been properly investigated in this work.

This study has assessed the overall efficiency of a micro-TPV combustor from three aspects. Although the electric power output was not high, the concept of the micro-CHP system fueled with bio-syngas was validified. The increase in CO concentration in fuel mixtures effectively improved the overall efficiency of the micro-CHP system, especially under fuel-rich conditions. Due to the micro-scale of the experiment, the total energy generated by the micro-CHP system could be insufficient for daily use. By enlarging the scale of micro-combustor, which means increasing the surface area of the emitter could increase the electricity produced by TPV system. Additionally, PV array could be upgraded or replaced by a lower-bandgap PV cell, such as InGaAsSb. Moreover, the simplicity of the present micro-CHP system is an advantage from the view point of manufacture. By enlarging the scale of the whole system, the idea of a distributed power generator could be materialized.

Author contribution

Wen-Lih Chen: Conceptualization, Supervision, Methodology, Data Analysis, Writing- Reviewing and Editing. Gaetano Currao: Data Analysis, Writing- Reviewing and Editing. Yueh-Heng Li: Conceptualization, Supervision, Methodology, Data Analysis, Writing- Original Draft Preparation, Writing- Reviewing and Editing. Chien-Chun Kao: Conducting Experiments, Data Curation, Data Analysis,

Declaration of competing interest

The authors declare that they have no known competing financial interests or personal relationships that could have appeared to influence the work reported in this paper.

Data availability

Data will be made available on request.

Acknowledgments

This work was financially supported by the Ministry of Science and Technology, Taiwan, under the grant numbers MOST 106-2923-E-006-003-MY3, MOST 108-2628-E-006-008-MY3, and MOST 109-2221-E-006-037-MY3.

References

[1] Lasek L, Głód K, Słowik K. The co-combustion of torrefied municipal solid waste and coal in bubbling fluidised bed combustor under atmospheric and elevated pressure. Renew Energy 2021;179:828–41.
[2] Kuo W-C, Lasek J, Słowik K, Głód K, Jagustyn B, Li Y-H, et al. Low-temperature pretreatment of municipal solid waste for efficient application in combustion systems. Energy Convers Manag 2019;196:525–35.
[3] Rizwan M, Saif Y, Almansoori A, Elkamel A. A multiobjective optimization framework for sustainable design of municipal solid waste processing pathways to energy and materials. Int J Energy Res 2020;44(2):771–83.
[4] Ravindran R, Jaiswal AK. Exploitation of food industry waste for high-value products. Trends Biotechnol 2016;34(1):58–69.
[5] Wang F, Jiang Y, Guo W, Niu K, Zhang R, Hou S, et al. An environmentally friendly and productive process for bioethanol production from potato waste. Biotechnol Biofuels 2016;9(1):1–10.
[6] Schlamadinger B, Apps M, Bohlin F, Gustavsson L, Jungmeier G, Marland G, et al. Towards a standard methodology for greenhouse gas balances of bioenergy systems in comparison with fossil energy systems. Biomass Bioenergy 1997;13(6):359–75.
[7] Sadaf S, Iqbal J, Ullah I, Bhatti HN, Nouren S, Nisar J, et al. Biodiesel production from waste cooking oil: an efficient technique to convert waste into biodiesel. Sustain Cities Soc 2018;41:220–6.
[8] Ware A, Power N. Biogas from cattle slaughterhouse waste: energy recovery towards an energy self-sufficient industry in Ireland. Renew Energy 2016;97:541–9.
[9] De Sales CAVB, Maya DMY, Lora EES, Jaén RL, Reyes AMM, González AM, et al. Experimental study on biomass (eucalyptus spp.) gasification in a two-stage downdraft reactor by using mixtures of air, saturated steam and oxygen as gasifying agents. Energy Convers Manag 2017;145:314–23.
[10] Ruiz JA, Juárez M, Morales M, Muñoz P, Mendívil M. Biomass gasification for electricity generation: review of current technology barriers. Renew Sustain Energy Rev 2013;18:174–83.
[11] Al-Attab K, Zainal Z. Micro gas turbine running on naturally aspirated syngas: an experimental investigation. Renew Energy 2018;119:210–6.
[12] Li Y-H, Kuo W-C. The study of optimal parameters of oxygen-enriched combustion in fluidized bed with optimal torrefied woody waste. Int J Energy Res 2020;44(9):7416–34.
[13] Basu S, Chen YB, Zhang Z. Microscale radiation in thermophotovoltaic devices—a review. Int J Energy Res 2007;31(6-7):689–716.
[14] Yablonovitch E. Inhibited spontaneous emission in solid-state physics and electronics. Phys Rev Lett 1987;58(20):2059.
[15] Nam Y, Yeng YX, Lenert A, Bermel P, Celanovic I, Soljačić M, et al. Solar thermophotovoltaic energy conversion systems with two-dimensional tantalum photonic crystal absorbers and emitters. Sol Energy Mater Sol Cell 2014;122:287–96.
[16] Balli O, Aras H. Energetic and exergetic performance evaluation of a combined heat and power system with the micro gas turbine (MGTCHP). Int J Energy Res 2007;31(14):1425–40.
[17] Wu C-Y, Currao GMD, Chen W-L, Chang C-Y, Hu B-Y, Wang T-H, et al. The application of an innovative integrated Swiss-roll-combustor/Stirling-hot-end component on an unpressurized Stirling engine. Energy Convers Manag 2021;249:114831.
[18] Bianchi M, De Pascale A, Spina PR. Guidelines for residential micro-CHP systems design. Appl Energy 2012;97:673–85.
[19] Chen M, Lund H, Rosendahl LA, Condra TJ. Energy efficiency analysis and impact evaluation of the application of thermoelectric power cycle to today's CHP systems. Appl Energy 2010;87(4):1231–8.
[20] Yin Y, Chen S, Li X, Jiang B, Zhao JR, Nong G. Comparative analysis of different CHP systems using biogas for the cassava starch plants. Energy 2021;232:121028.
[21] Chen Z, Yiliang X, Hongxia Z, Yujie G, Xiongwen Z. Optimal design and performance assessment for a solar powered electricity, heating and hydrogen integrated energy system. Energy 2023;262:125453.
[22] Shakeel MR, Mokheimer EMA. A techno-economic evaluation of utility scale solar power generation. Energy 2022;261:125170.
[23] Li Y-H, Kao W-C. Taguchi optimization of solar thermal and heat pump combisystems under five distinct climatic conditions. Appl Therm Eng 2018;133:283–97.
[24] Modi A, Bühler F, Andreasen JG, Haglind F. A review of solar energy based heat and power generation systems. Renew Sustain Energy Rev 2017;67:1047–64.
[25] Wu J, Han Y. Integration strategy optimization of solar-aided combined heat and power (CHP) system. Energy 2023;263:125875.
[26] Li Y-H, Hong JR. Power generation performance of hydrogen-fueled micro thermophotovoltaic reactor. Int J Hydrogen Energy 2018;43(3):1459–69.
[27] Li Y-H, Hong J-R. Performance assessment of catalytic combustion-driven thermophotovoltaic platinum tubular reactor. Appl Energy 2018;211:843–53.
[28] Li Y-H, Wu C-Y, Li H-Y, Chao Y-C. Concept and combustion characteristics of the high-luminescence flame for thermophotovoltaic systems. Proc Combust Inst 2011;33(2):3447–54.
[29] Chirumamilla M, Roberts AS, Ding F, Wang D, Kristensen PK, Bozhevolnyi SI, et al. Multilayer tungsten-alumina-based broadband light absorbers for high-temperature applications. Opt Mater Express 2016;6(8):2704–14.
[30] Li Y-H, Wu C-Y, Lien Y-S, Chao Y-C. Development of a high-flame-luminosity thermophotovoltaic power system. Chem Eng J 2010;162(1):307–13.
[31] Li Y-H, Kao H-H, Wang Y-R, Wan J, Manatura K. Performance optimizing and entropy generation analysis of a platinum–stainless-steel segmented microreactor. Chem Eng J 2023;457:141151.
[32] Yeng YX, Chou JB, Rinnerbauer V, Shen Y, Kim S-G, Joannopoulos JD, et al. Global optimization of omnidirectional wavelength selective emitters/absorbers based on dielectric-filled anti-reflection coated two-dimensional metallic photonic crystals. Opt Express 2014;22(18):21711–8.
[33] Qiu K, Hayden A. Development of a novel cascading TPV and TE power generation system. Appl Energy 2012;91(1):304–8.
[34] Qiu K, Hayden A. Implementation of a TPV integrated boiler for micro-CHP in residential buildings. Appl Energy 2014;134:143–9.
[35] Huang C-W, Li Y-H, Xiao K-L, Lasek J. Cofiring characteristics of coal blended with torrefied Miscanthus biochar optimized with three Taguchi indexes. Energy 2019;172:566–79.
[36] Comakli K, Simsek F, Comakli O, Sahin B. Determination of optimum working conditions R22 and R404A refrigerant mixtures in heat-pumps using Taguchi method. Appl Energy 2009;86(11):2451–8.
[37] Coşkun S, Motorcu AR, Yamankaradeniz N, Pulat E. Evaluation of control parameters' effects on system performance with Taguchi method in waste heat

recovery application using mechanical heat pump. Int J Refrig 2012;35(4):795–809.
[38] Salomons S, Hayes R, Votsmeier M. The promotion of carbon monoxide oxidation by hydrogen on supported platinum catalyst. Applied Catalysis A: General. 2009;352(1–2):27–34.
[39] Li Y-H, Chen G-B, Wu F-H, Cheng T-S, Chao Y-C. Effects of catalyst segmentation with cavities on combustion enhancement of blended fuels in a micro channel. Combust Flame 2012;159(4):1644–51.
[40] Chen W-L, Huang C-W, Li Y-H, Kao C-C, Cong HT. Biosyngas-fueled platinum reactor applied in micro combined heat and power system with a thermophotovoltaic array and stirling engine. Energy 2020;194:116862.
[41] Wu Y-T, Li Y-H. Combustion characteristics of a micro segment platinum tubular reactor with a gap. Chem Eng J 2016;304:485–92.
[42] Taguchi G. Introduction to quality engineering: designing quality into products and processes. 1986.
[43] Naik AB, Reddy AC. Optimization of tensile strength in TIG welding using the Taguchi method and analysis of variance (ANOVA). Therm Sci Eng Prog 2018;8:327–39.
[44] Taniguchi H, Mouri K, Nakahara T, Arai N. Exergy analysis on combustion and energy conversion processes. Energy 2005;30(2–4):111–7.
[45] Wu Y, Yang W, Blasiak W. Energy and exergy analysis of high temperature agent gasification of biomass. Energies 2014;7(4):2107–22.
[46] Martínez I. Lectures on Thermodynamics. 1992.
[47] Zanchini E, Terlizzese T. Molar exergy and flow exergy of pure chemical fuels. Energy 2009;34(9):1246–59.
[48] Chen G-L, Chen G-B, Li Y-H, Wu W-T. A study of thermal pyrolysis for castor meal using the Taguchi method. Energy 2014;71:62–70.
[49] Li Y-H, Chen G-B, Lin Y-C, Chao YC. Effects of flue gas recirculation on the premixed oxy-methane flames in atmospheric condition. Energy 2015;89:845–57.
[51] Li Y-H, Hsu H-W, Lien Y-S, Chao Y-C. Design of a novel hydrogen-syngas catalytic mesh combustor. Int J Hydrogen Energy 2009;34(19):8322–8.
[52] Li Y-H, Cheng T-T, Lien YS, Chao YC. Development of a tubular flame combustor for thermophotovoltaic power systems. Proc Combus Inst 2011;33(2):3439–45.